Tuning near field radiation by doped silicon

Jiawei Shi, Pengfei Li, Baoan Liu, and Sheng Shen

Citation: Applied Physics Letters **102**, 183114 (2013); doi: 10.1063/1.4804631
View online: http://dx.doi.org/10.1063/1.4804631
View Table of Contents: http://scitation.aip.org/content/aip/journal/apl/102/18?ver=pdfcov
Published by the AIP Publishing

Tuning near field radiation by doped silicon

Jiawei Shi, Pengfei Li, Baoan Liu, and Sheng Shen[a)]
Department of Mechanical Engineering, Carnegie Mellon University, Pittsburgh, Pennsylvania 15213, USA

(Received 21 March 2013; accepted 27 April 2013; published online 9 May 2013)

In this letter, we demonstrate theoretically and experimentally that bulk silicon can be employed to overcome the challenge of tuning near field radiation. Theoretical calculation shows that the nanoscale radiation between bulk silicon and silicon dioxide can be tuned by changing the carrier concentration of silicon. Near field radiation measurements are carried out on multiple bulk silicon samples with different doping concentrations. The measured near field conductance agrees well with theoretical predictions, which demonstrates a tuning range from 2 nW/K to 6 nW/K at a gap of ~60 nm. © *2013 AIP Publishing LLC*. [http://dx.doi.org/10.1063/1.4804631]

Since the significant enhancement of radiative heat transfer was observed in the near field,[1–4] control of near field radiative heat transfer (NFRHT) has attracted intense interests. It has been theoretically predicted that NFRHT can be controlled using nanoporous materials,[5] thin films,[6,7] and graphene sheets,[8–11] or by adjusting the material temperature,[12] surface roughness,[13] and metal-insulator transition.[14] In contrast to a large number of theoretical studies, there exist few experiments that demonstrate the tuning of NFRHT. The initial experiment has recently been carried out based on tuning the metal-insulator transition in phase change materials.[15]

One unique characteristic of doped semiconductors is that their plasma frequency can be tuned by modifying the carrier concentration. Theoretical calculations have shown that doping concentration dramatically affects NFRHT between two parallel semi-infinite doped silicon at different temperatures.[16,17] Very recently, van Zwol *et al*. measured NFRHT between a glass microsphere and two thin silicon films with different carrier concentrations, but detailed theoretical analysis was not provided, and the trend of NFRHT versus carrier concentration was still unclear as only two samples were measured.[11] In this letter, we provide a comprehensive analysis for tuning NFRHT through changing the carrier concentration of both p-type and n-type bulk silicon. To fully demonstrate the tunability of NFRHT using doped silicon and to verify our theoretical results, measurements of NFRHT are conducted towards multiple bulk silicon samples with different carrier concentrations.

At thermal equilibrium, the fluctuation of electrons or ions in materials induces random currents, which radiate electromagnetic waves to the surroundings.[18] For instance, the radiation from a medium to vacuum can be divided into three modes by comparing the values of β and k_0.[19] Here, β denotes the component of wave vector parallel to the interface between the medium and vacuum, k_0 denotes the wave vector in vacuum. When $\beta < k_0$, there are propagating waves on both sides of the interface, which are responsible for the far field thermal radiation from the medium. When $k_0 < \beta < nk_0$, where n represents the refractive index of the medium, total internal reflection occurs, resulting in propagating waves inside the medium and evanescent waves outside the medium. When $\beta > nk_0$, there exist evanescent waves on both sides of the interface. In this case, resonant surface waves can be excited when Re(ε) is negative and Im(ε) is sufficiently small, where ε is the permittivity of the medium. Since the dielectric function of doped silicon cannot meet both conditions simultaneously, it is difficult to excite resonant surface plasmons in doped silicon.[17] But evanescent waves can still exist and contribute to the near field radiation. Therefore, it is the second and third radiation modes that lead to the strong enhancement of radiative heat transfer of doped silicon in the near field.

Fluctuation dissipation theorem (FDT) and Green's tensor are widely employed to calculate the radiative response from a body in the near field.[18,20] The FDT describes the statistical properties of random currents, while the Green's tensor enables us to calculate the electromagnetic response for a given geometry. In our calculation, all the materials are assumed to be isotropic and non-magnetic. The Drude model is used to describe the dielectric function of doped silicon,[17]

$$\epsilon(\omega) = \epsilon_{bl} - \frac{N_e e^2/\epsilon_0 m_e^*}{\omega^2 + i\omega/\tau_e} - \frac{N_h e^2/\epsilon_0 m_h^*}{\omega^2 + i\omega/\tau_h}, \quad (1)$$

where the first term on the right hand side ϵ_{bl} represents the dielectric function of intrinsic silicon.[21] The second term is the Drude term for transitions in the conduction band (free electrons). The third term is the Drude term for transitions in the valence band (free holes). N_e and N_h are carrier concentrations for electrons and holes, m_e^* and m_h^* are effective masses of electrons and holes for conductivity calculation, and τ_e and τ_h are scattering times for free electrons and holes, respectively. Here, we take the values of effective mass as $m_e^* = 0.27m_0$ and $m_h^* = 0.37m_0$, where m_0 is free electron mass.[17]

It can be seen from Eq. (1) that it is necessary to first determine carrier concentrations (N_e and N_h) and scattering times (τ_e and τ_h) in order to obtain a proper expression for $\epsilon(\omega)$. When the doping concentration is low, complete ionization can be achieved. However, when the doping concentration is very high ($>10^{19}$/cm^3), the dopants cannot be completely ionized. In this calculation, a general analysis is applied to account for both complete and incomplete

[a)]Email: sshen1@cmu.edu

ionizations based on charge neutrality.[22] This method is valid for both non-degenerately and degenerately doped silicon. Although scattering time is the most important parameter in the Drude model, it is difficult to calculate directly. The scattering time used here is extracted from the empirical expression for mobility.[23] In the present work, both carrier concentration and scattering time are determined by Hall effect measurements, which enables us to directly compare theoretical calculations with experimental measurements.

Using the Green's tensor and FDT, the LDOS of photons in the vicinity of SiO_2 and doped silicon surfaces can be calculated.[20] Figures 1(a) and 1(b) show the LDOS at a distance of 50 nm from the surfaces of arsenic-doped n-type silicon and boron-doped p-type silicon, respectively. The black curve with sharp peaks represents the LDOS at a distance of 50 nm from the surface of SiO_2. There also exists a peak in the LDOS spectrum for doped silicon. Moreover, the peak can be shifted through modifying its carrier concentration. As shown in Fig. 1(a), when the carrier concentration is low, the peak is located at low frequencies. In this case, there is no overlap between the LDOS peaks of doped silicon and SiO_2, indicating a weak coupling between these two materials. As carrier concentration increases, the peak of doped silicon moves towards higher frequencies. The strongest enhancement of NFRHT between SiO_2 and doped silicon occurs when the peak of doped silicon overlaps with the strongest peak of SiO_2. The corresponding carrier concentration of n-type doped silicon is around $1.5 \times 10^{19}/cm^3$, as shown by the red curve in Fig. 1(a). Figure 1(b) shows the evolution of the LDOS peak of p-type silicon versus carrier concentration. All the peaks of LDOS for p-type silicon shows a red shift for the same carrier concentrations, compared with n-type silicon. This is attributed to the difference of effective mass and scattering time between electrons and holes.

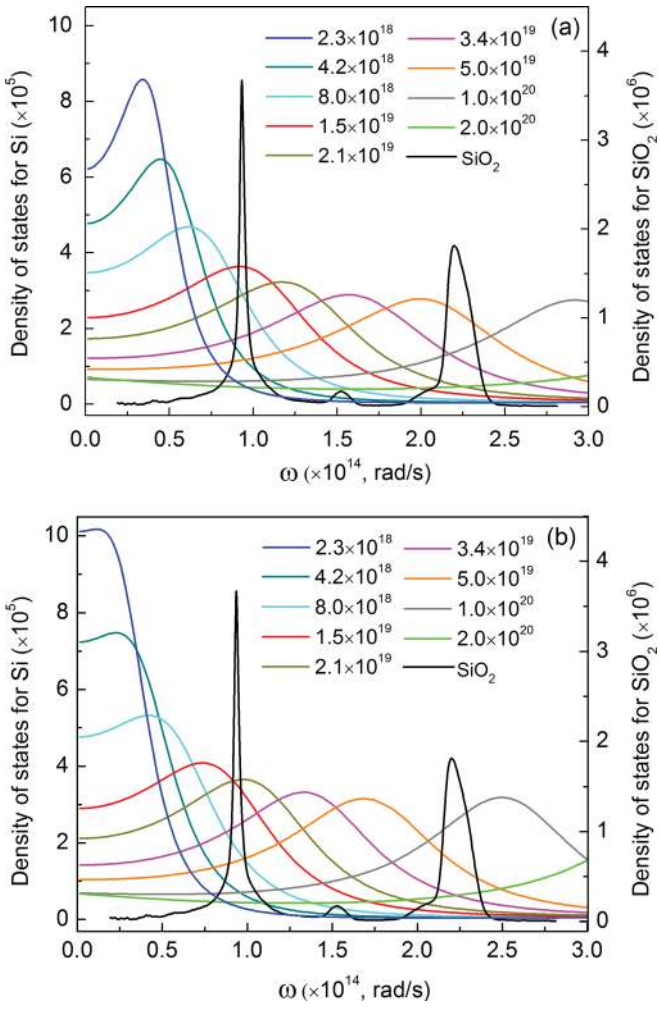

FIG. 1. (a) Local density of states at a distance of 50 nm from the surfaces of SiO_2 (black curve) and arsenic-doped n-type silicon (all other curves) with different carrier concentrations (unit, $/cm^3$). (b) Local density of states at a distance of 50 nm from the surfaces of SiO_2 (black curve) and boron-doped p-type silicon (all other curves) with different carrier concentrations (unit, $/cm^3$).

Experimental details have been described in our previous publications.[24] Here, we only introduce several key points. To prepare the probe, a glass microsphere (Microspheres-Nanospheres) with a diameter of $\sim 100\,\mu m$ (Fig. 2(a)) is attached onto the tip of a bi-material rectangle cantilever using silver epoxy, as shown in Fig. 2(b).[25] The surface roughness of the microsphere is required to be as small as possible in order to clearly define a nanoscale gap between the microsphere and the sample. The one dimensional (1D) roughness of the microsphere surface is measured to be ~ 4 nm (Fig. 3(c)). All bulk silicon samples are aligned along the edge of a copper plate and then loaded

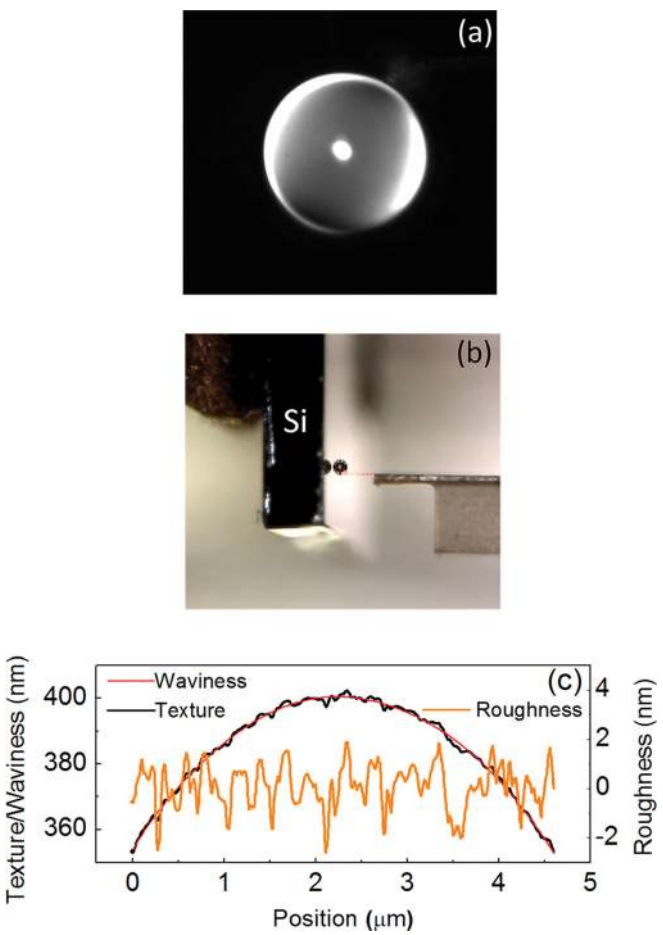

FIG. 2. (a) The optical image of the microsphere. (b) The relative position between a bulk silicon sample and the probe. (c) The 1D roughness (the orange curve) is obtained by subtracting the 1D waviness (the red curve) from the 1D texture (the black curve) of the microsphere surface.

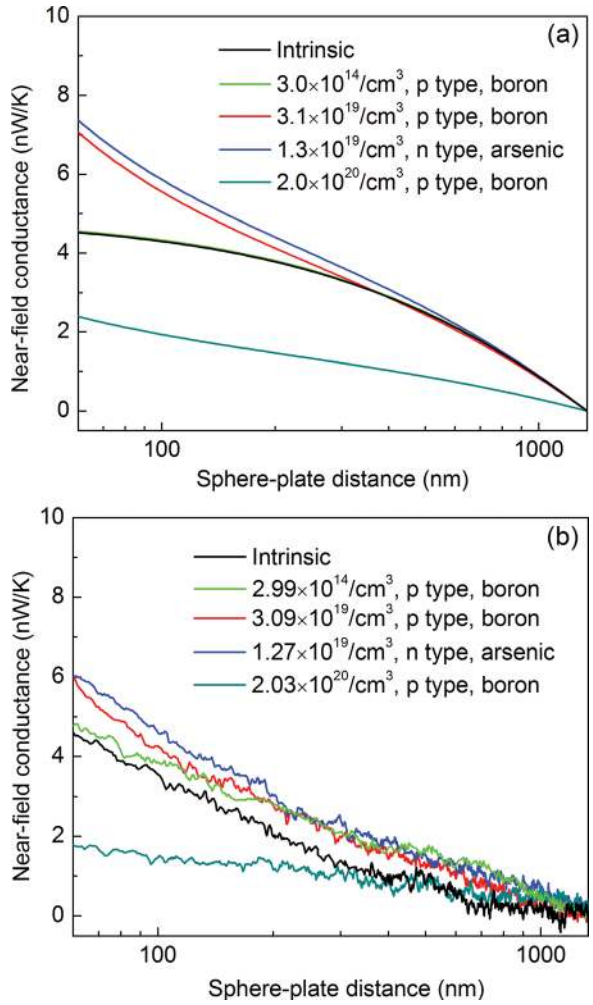

FIG. 3. (a) Calculated near field conductance curves corresponding to the five bulk silicon samples at different carrier concentrations. (b) Measured near field conductance curves corresponding to the five bulk silicon samples. The measurement uncertainty is estimated to be ~0.5 nW/K in terms of the noise level of deflection signals, the error in cantilever calibration, etc.

onto a 3D piezoelectric translation stage (MadCity Labs) with a step resolution of 1 nm. The piezoelectric translation stage is placed on a motorized 3D micromanipulator with a traveling distance of 25 mm in all three axes (Sutter Instrument). During our measurements, the samples can be switched conveniently by changing the height of the sample loader using the micromanipulator. The heat flow radiated by the microsphere greatly increases due to the enhancement of NFRHT when the sphere approaches the sample. The resulting temperature change of the cantilever causes its bending. The deflection of the cantilever at the tip is monitored using an optical deflection system. The entire setup is placed on a mechanical vibration isolator, and the measurement is conducted under a vacuum level of $\sim 1 \times 10^{-6}$ Torr.

TABLE I. Hall effect measurements of five different samples.

Sample	Carrier concentration	Mobility	Bulk resistivity	Type
1	$1.31 \times 10^{11}/cm^3$	1770 $cm^2/V{\cdot}s$	2.71×10^4 Ω·cm	Intrinsic
2	$2.99 \times 10^{14}/cm^3$	1960 $cm^2/V{\cdot}s$	10.6499 Ω·cm	p, boron
3	$3.09 \times 10^{19}/cm^3$	59.7 $cm^2/V{\cdot}s$	0.0033 Ω·cm	p, boron
4	$1.27 \times 10^{19}/cm^3$	114.2 $cm^2/V{\cdot}s$	0.0043 Ω·cm	n, arsenic
5	$2.03 \times 10^{20}/cm^3$	45.4 $cm^2/V{\cdot}s$	0.0007 Ω·cm	p, boron

Five bulk silicon samples with different carrier concentrations are measured to demonstrate the tunability of near-field conductance. Considering the difference between the electron and hole mobilities, an n-type doped silicon sample is also included. The carrier concentrations and the mobilities of all five samples are determined by Hall effect measurements, as shown in Table I. The surface charges on the microsphere and the sample are minimized by contacting them with a grounded copper plate before measurement so that the electrostatic force can be well suppressed. The near field conductance between the microsphere and the samples is calculated using the Derjaguin approximation.[3] In Fig. 3(a), starting from the intrinsic silicon (black curve), the near field conductance of p-type doped silicon increases with the increase of carrier concentration from $3.0 \times 10^{14}/cm^3$ (green curve) to $3.0 \times 10^{19}/cm^3$ (red curve). However, if the carrier concentration is too high, e.g., $2.0 \times 10^{20}/cm^3$, the near field conductance drops dramatically (cyan curve). This is because the peak of LDOS for doped silicon significantly deviates from the surface phonon polariton resonance peaks of SiO_2 at such a high carrier concentration (Fig. 1(b)).

In our experiments, the directly measured signal is the deflection of the cantilever, which can be further calibrated to obtain the near field conductance.[26,27] Figure 3(b) shows the measured near field conductances for the five samples. The black curve is the measured near field conductance for the intrinsic silicon. For the p-type samples with carrier concentration of $2.99 \times 10^{14}/cm^3$ (green curve) and $3.09 \times 10^{19}/cm^3$ (red curve), the near field conductance is higher than that of the intrinsic silicon due to the contribution from free carriers. When the carrier concentration is as high as $2.03 \times 10^{20}/cm^3$ for p-type samples, a large decrease in the near field conductance is observed, as predicted in Fig. 3(a). For the n-type sample with a carrier concentration of $1.27 \times 10^{19}/cm^3$ (blue curve), an enhancement of near field conductance beyond intrinsic silicon is also observed, which is consistent with the prediction in Fig. 3(a). At a gap of ~60 nm, near-field conductance can be dramatically tuned from 2 nW/K to 6 nW/K by changing the doping concentration of silicon.

In summary, doped silicon has been utilized to control the NFRHT. We theoretically show that the NFRHT between doped silicon and silicon dioxide can be significantly tuned by changing the carrier concentration of silicon. Our experimental results for both n-type and p-type silicon samples agree well with theoretical predictions. The tunable near field thermal conductance may shed light on the development of thermophotovoltaic devices and advanced thermal management systems.

The authors would like to thank Professors Robert Davis and Elias Towe for helpful discussions, and Yao Yao, Yuhan Liang, and Jacob Melby for their assistance with Hall effect measurements. This work is supported by the Carnegie Mellon University start-up fund and the National Science Foundation (CBET-1253692).

[1]A. Kittel, W. Müller-Hirsch, J. Parisi, and S.-A. Biehs, Phys. Rev. Lett. **95**, 224301 (2005).

[2]S. Shen, A. Narayanaswamy, and G. Chen, Nano Lett. **9**, 2909 (2009).
[3]E. Rousseau, A. Siria, G. Jourdan, S. Volz, F. Comin, J. Chevrier and J.-J. Greffet, Nat. Photonics **3**, 514 (2009).
[4]R. S. Ottens, V. Quetschke, S. Wise, A. A. Alemi, R. Lundock, G. Mueller, D. H. Reitze, D. B. Tanner, and B. F. Whiting, Phys. Rev. Lett. **107**, 014301 (2011).
[5]S.-A. Biehs, P. Ben-Abdallah, F. S. S. Rosa, K. Joulain, and J.-J. Greffet, Opt. Express **19**, A1088 (2011).
[6]M. Francoeur, M. P. Mengüç, and R. Vaillon, Appl. Phys. Lett. **93**, 043109 (2008).
[7]S. Basu and M. Francoeur, Appl. Phys. Lett. **98**, 113106 (2011).
[8]O. Ilic, M. Jablan, J. D. Joannopoulos, I. Celanovic, H. Buljan, and M. Soljačić, Phys. Rev. B **85**, 155422 (2012).
[9]V. B. Svetovoy, P. J. van Zwol, and J. Chevrier, Phys. Rev. B **85**, 155418 (2012).
[10]A. I. Volokitin and B. N. J. Persson, Phys. Rev. B **83**, 241407 (2011).
[11]P. J. van Zwol, S. Thiele, C. Berger, W. A. de Heer, and J. Chevrier, Phys. Rev. Lett. **109**, 264301 (2012).
[12]C. R. Otey, W. T. Lau, and S. Fan, Phys. Rev. Lett. **104**, 154301 (2010).
[13]S.-A. Biehs and J.-J. Greffet, Phys. Rev. B **82**, 245410 (2010).
[14]P. J. van Zwol, K. Joulain, P. Ben-Abdallah, and J. Chevrier, Phys. Rev. B **84**, 161413 (2011).
[15]P. J. van Zwol, L. Ranno, and J. Chevrier, Phys. Rev. Lett. **108**, 234301 (2012).
[16]F. Marquier, K. Joulain, J. P. Mulet, and R. Carminati, J.-J. Greffet, Opt Commun. **237**, 379 (2004).
[17]C. J. Fu and Z. M. Zhang, Int. J. Heat Mass Transfer **49**, 1703 (2006).
[18]S. M. Rytov, *Theory of Electric Fluctuations and Thermal Radiation* (Air Force Cambridge Research Center, Bedford, MA, 1959).
[19]S.-A. Biehs, E. Rousseau, and J.-J. Greffet, Phys. Rev. Lett. **105**, 234301 (2010).
[20]K. Joulain, J.-P. Mulet, F. Marquier, R. Carminati, and J.-J. Greffet, Surf. Sci. Rep. **57**, 59 (2005).
[21]D. F. Edwards, Silicon (Si), in *Handbook of Optical Constants of Solids*, edited by E. D. Palik (Academic Press, New York, 1998), Vol. 1, pp. 547–570.
[22]T. K. Gaylord and J. N. Linxwiler Jr., Am. J. Phys. **44**, 353 (1976).
[23]W. E. Beadle, J. C. C. Tsai, and R. D. Plummer, *Quick Reference Manual for Silicon Integrated Circuit Technology* (John Wiley & Sons, NewYork, 1985), Chapters 1 and 2.
[24]A. Narayanaswamy, S. Shen, and G. Chen, Phys. Rev. B **78**, 115303 (2008).
[25]J. R. Barnes, R. J. Stephenson, C. N. Woodburn, S. J. O'Shea, M. E. Welland, T. Rayment, J. K. Gimzewski, and Ch. Gerber, Rev. Sci. Instrum. **65**, 3793 (1994).
[26]S. Shen, A. Narayanaswamy, S. Goh, and G. Chen, Appl. Phys. Lett. **92**, 063509 (2008).
[27]A. Narayanaswamy and N. Gu, J. Heat Transfer **133**, 042401 (2011).